REVIEW

A Perspective on Enzyme Catalysis

Stephen J. Benkovic* and Sharon Hammes-Schiffer*

The seminal hypotheses proposed over the years for enzymatic catalysis are scrutinized. The historical record is explored from both biochemical and theoretical perspectives. Particular attention is given to the impact of molecular motions within the protein on the enzyme's catalytic properties. A case study for the enzyme dihydrofolate reductase provides evidence for coupled networks of predominantly conserved residues that influence the protein structure and motion. Such coupled networks have important implications for the origin and evolution of enzymes, as well as for protein engineering.

The fascinating catalytic process executed by enzymes has long remained a mystery. How do enzymes achieve accelerated rates for difficult chemical transformations and exquisite specificity toward substrates distinguished only by their stereochemistry? Here, we review proffered hypotheses, supportive and occasionally counterintuitive experiments, and our current level of understanding or ignorance. As with any summary, the choice of material reflects our own biases, and doubtless other choices might easily have sufficed. In particular, we look at the question of how molecular motions within the protein's structure may influence the enzyme's catalytic properties.

The Historical Record

Biochemical perspective. Much has been written about the historical exploration of enzymatic catalysis. Among the first hypotheses offered are the familiar "lock and key" model (*1*), which proposed that the binding of a substrate molecule to the active site on the enzyme results in activation of the substrate (in modern terms, a reactive conformation), and a later modified version in which the "key does not quite fit the lock perfectly but exercises a certain strain on it" (*2*) (in modern terms, ground-state destabilization). With the advent of transition-state theory, the hypothesis of enzyme–transition-state complementarity (*3*), which found a preferential binding of the transition state rather than the substrate or product as the source of catalysis, took center stage. This prediction was neatly satisfied by the first enzyme structure solved, that of lysozyme, with the polysaccharide $(N\text{-acetylglucosamine})_3$ bound at its active site. The structure showed the transition state for glycoside cleavage to be stabilized by the enzyme: The strong electrostatic field of the two carboxylates contributed by Asp^{52} and Glu^{35} on either side of the active-site cleft are positioned to interact with the developing positive charge on the oxocarbenium ion (Fig. 1) (*4*–*6*).

The comparison of enzyme-catalyzed and noncatalytic rates has provided an estimate of the degree of enzymatic transition-state stabilization. Careful measurements of the rates for spontaneous hydrolysis of ionized phosphate monoesters and diesters relative to *Escherichia coli* alkaline phosphatase (*7*) or staphylococcal nuclease acting on the same substrate reveals that these enzymes enhance the rates of the hydrolysis reaction by 10^{15}-fold to 10^{17}-fold. These values are at the upper end of rate enhancements [a more extensive tabulation can be found in (*8*)] and provide a measure of what is meant by a catalytic process. Applying transition-state theory, the rates have been used to calculate the hypothetical binding of a transition state to its enzyme through the pseudothermodynamic cycle shown in Scheme 1, where $K_{TS} = k_{NON}/k_{cat}/K_M$. The resulting affinities can be astonishingly high (e.g., $K_{TS} = 10^{-24}$ M in the case of the enzymic decarboxylation of orotic acid), but the interpretation of this calculation (*9*) is subject to a number of uncertainties primarily rooted in the obvious environmental differences between a transition state in an aqueous solvent shell and one surrounded by the amino acid walls of an active-site cavity.

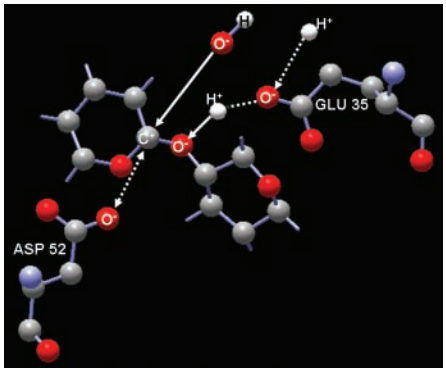

Fig. 1. Schematic picture of the transition-state stabilization in lysozyme. The oxocarbenium ion is stabilized by interactions with Asp^{52} and Glu^{35} (*6*, *119*).

In this picture of catalysis, which takes advantage of thermodynamic state function descriptors of the free energy of activation (*10*) for the substrate and transition states, enzymic catalytic power will always appear as a result of increased transition-state stabilization (lower free energy) for the enzymic process relative to the reference reaction. How it is parceled among specific forces (*11*, *12*) between the substrate and enzyme, i.e., electrostatic, steric, hydrogen-bonding, or differential solvation effects, is not specified. As a consequence, there has been an increased scrutiny of how the binding interactions arising from favorable and unfavorable noncovalent bonding between the reactants and residues within the active site are translated into catalysis (*13*–*14*).

Parallel to the appearance of x-ray crystallographic structures of enzymes was the advent of numerous physical organic studies on various model systems that mimicked active-site features (*15*). The details of general acid-base and nucleophilic catalysis for acyl transfer reactions and glycoside and acetal hydrolysis highlighted the possibility of stepwise or concerted proton transfers to and from metastable intermediates or transition states with chemical entities such as amines, imidazoles, and carboxylates, which function in the active site. These studies (*16*, *17*) provided fresh insights into the chemical identity of species along the reaction coordinate that link ground and transition states.

Similarly, physical organic experiments in which a given chemical reaction was performed in various solvents, generally ranging

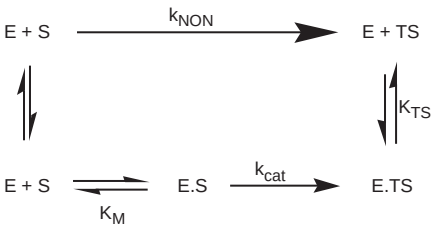

Scheme 1

Department of Chemistry, 152 Davey Laboratory, Pennsylvania State University, University Park, PA 16802, USA.

*To whom correspondence should be addressed. E-mail: sjb1@psu.edu (S.J.B.) and shs@chem.psu.edu (S.H.S.)

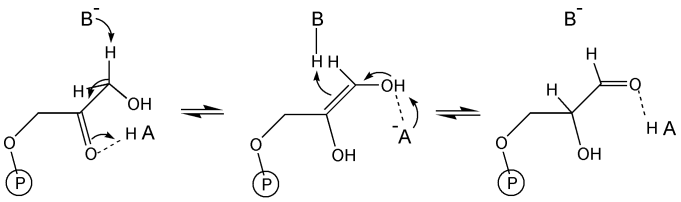

Fig. 2. The reaction catalyzed by triosephosphate isomerase. The reactant is DHAP (dihydroxyacetone phosphate), and the product is GAP (glyceraldehyde 3-phosphate). The catalytic basic group is denoted B, and the catalytic acidic group is denoted HA (*23*).

from aprotic to protic, showed especially for many S_N2 displacement reactions that the effect of solvent is to retard the rate relative to what would be observed for this reaction under the same conditions in the gas phase. Extrapolation to the low dielectic typical of an enzyme's active-site cavity (*18*) prompted early proposals that enzymes act through a desolvation mechanism (*19*–*21*). Alternatively, the effect may be described as solvent substitution, with the active-site residues furnishing a polar framework to replace the solvating water molecules (*22*).

Collectively, these experiments suggest that enzymatic catalysis could be understood in terms of physical organic principles. One striking feature, seen repeatedly, is that the catalytic elements in an active site are precisely positioned for their function. A beautiful, early example is furnished by the enzyme triosephosphate isomerase, which catalyzes the interconversion of glyceraldehyde 3-phosphate and dihydroxyacetone phosphate through a cis enediol intermediate assisted by general acid-base catalysis (Fig. 2). From kinetic, stereochemical, chemical modification, and site-specific mutagenesis experiments, B had been identified as Glu^{165} and HA as His^{95} (*23*). The crystal structure (Fig. 3) with either a substrate or substrate analog showed that arrangement of substrate relative to the catalyzing residues was indeed one of remarkable precision: The carboxylate is within 3 Å of enediol carbons, requiring minimal motion of the bidentate carboxylate to shuttle the proton, and the His^{95} is within 3 Å of the substrate oxygens, allowing it to donate a proton (*24*). [For further ramifications of the positioning, see (*23*).] The above precision facilitates passage through the transition state and thus provides a more satisfying picture of what might be meant by transition-state stabilization.

But how is this alignment achieved? Investigations that compared the rate constants for intramolecular and intermolecular reactions proceeding through a common mechanism (for example, anhydride formation) showed that intramolecular reactions exhibit rate enhancements of 10^3 to 10^6 (*25*). Extrapolating this to enzymes, many have argued (although the nomenclature and descriptions are not identical) that the preorganization of an enzyme's active site allows the selection of subpopulations of the substrate ensemble that approach the configuration of the relevant transition state and are bound with high affinity (*13*). This is achieved through the energy of binding and the imposition of steric and nonbonding interactions within the active-site cavity (*26*). Molecular dynamics simulations suggest that this population [sometimes referred to as near-attack conformations or NACs, whose ligand distances/angles are defined for a given system on the basis of its computed transition state (*27*)] can be significant, for example, approaching 50% for the configuration of substrate and cofactor at the active site of lactate dehydrogenase. Thus, it is conceivable that many enzyme-substrate (ES) complexes have a fair fraction of their populations close to the transition structure. Other computational studies suggest that steric effects (defined as nonelectrostatic strain) are not the main components of enzyme catalysis, but rather that electrostatic effects are responsible for most of the catalysis (i.e., the enzyme reduces the electrostatic reorganization free energy) (*22*, *28*). A more general perspective is that a combination of steric and electrostatic interactions work together to align the substrate, cofactor, and catalytic elements of the active site.

To achieve such ES complexes, as well as the precise alignments in the transition state necessary for efficient catalysis, transient reorganizations of the active site or more distal regions of the protein are often required. There are numerous instances of conformation changes in which loop elements (triose phosphate isomerase) or entire domains (RNA polymerase) move for 7 Å or 18 Å to sequester the substrate or to create a tunnel for an extruded polymeric product, preventing its dissociation (*29*). Alternatively, the binding of substrate induces an active conformation of the enzyme (induced fit) (*30*). These movements probably also act to provide the precise juxtapositioning of substrate and active-site residues. The time scales of various dynamic events that can occur in an enzyme complex are listed in Table 1. Because of the large number of degrees of freedom in macromolecules that dissipate kinetic energy, a mechanism of machinelike motions to provide energy to mount the catalytic barrier is unlikely. Alternative hypotheses for ways in which motion may aid catalysis will now be discussed.

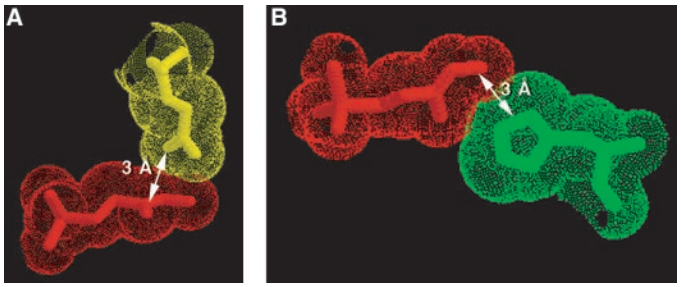

Fig. 3. Illustration of the precise fit among the catalytic elements of triosephosphate isomerase. (**A**) The fit between the substrate (red) and the catalytic base Glu^{165} (yellow). (**B**) The fit between the substrate (red) and the catalytic electrophile His^{95} (green) (*23*).

Table 1. The time scales of various dynamic events that can occur in an enzyme complex (*10*, *120*, *121*).

Motion	Approximate time scale log(s)
Bond vibration	−14 to −13
Proton transfer	−12
Hydrogen bonding	−12 to −11
Elastic vibration of globular region	−12 to −11
Sugar repuckering	−12 to −9
Rotation of side chains at surface	−11 to −10
Torsional libration of buried groups	−11 to −9
Hinge bending at domain interfaces	−11 to −7
Water structure reorganization	−8
Helix-coil breakdown/formation	−8 to −7
Allosteric transitions	−5 to 0
Local denaturation	−5 to 1
Rotation of medium-sized side chains in interior	−4 to 0

Theoretical perspective. Let us step back and look at enzymatic catalysis from the theoretical perspective. In general, chemical reactions are adiabatic, nonadiabatic, or in the intermediate regime [terminology defined in (*31*)]. The overall rate for an adiabatic chemical reaction in solution or protein may be expressed as the product of an equilibrium transition-state theory rate, which depends exponentially on the activation free-energy barrier, and a transmission coefficient prefactor, which accounts for dynamical recrossings of the barrier (*32*). Often the term "dynamical" is reserved for properties influencing the transmission coefficient, which is between zero and unity. Typically, the transmission coefficient does not have a substantial effect on the overall rate for chemical

reactions in solution (*33*). Analytical rate expressions for nonadiabatic reactions have been derived with perturbative Golden Rule approaches (*34*–*36*). The basic forms of the adiabatic and nonadiabatic rate expressions are analogous, despite the fundamental differences outlined in (*37*). Thus, the concepts underlying transition-state theory provide a useful framework for analyzing general enzymatic reactions.

Although enzyme systems involve the motions of many atoms, typically the free-energy profile is projected onto a single collective reaction coordinate, and the transition state is identified with the configuration at the top of the free-energy barrier (*38*). On the basis of fundamental reaction rate theory, enzymatic catalysis may be analyzed in terms of effects on the free-energy barrier and the transmission coefficient relative to the reaction in solution. Because the transmission coefficient is a prefactor, whereas the free-energy barrier is in the exponential of the overall rate expression, the most important contributions to enzymatic catalysis are expected to arise from the lowering of the free-energy barrier rather than from dynamical effects on the transmission coefficient. Computer simulations have supported this hypothesis and indicate that the reduction of the free-energy barrier by electrostatic effects is a major component of catalysis (*39*). The folded enzyme is thought to provide a preorganized polar environment that is already partially oriented to stabilize the transition state (*39*).

The catalytic role of enzymatic motions may be analyzed within this fundamental framework. Motions influencing the activation free-energy barrier are thermally averaged, equilibrium properties of the system, whereas motions influencing the transmission coefficient are dynamical properties of the system. Some motions may influence both the activation free-energy barrier and the transmission coefficient. Motions influencing the activation free-energy barrier are expected to have a greater catalytic role than those influencing the transmission coefficient, because the free-energy barrier is in the exponential whereas the transmission coefficient is a prefactor in the rate expression. Numerous computational studies have identified the importance of conformational changes in enzyme reactions (*14*, *40*–*57*). Some of these studies suggest that the binding of the substrate(s) modulates the distribution of conformations (*27*, *42*), and others suggest that specific modes of the protein are directly coupled to the chemical reaction (*49*, *51*, *58*). Recent theoretical studies indicate that thermally averaged, equilibrium motions representing conformational changes along the collective reaction coordinate play an important role in enzymatic reactions (*55*, *59*–*61*). These motions are averaged over the fast vibrations of the enzyme and occur on the time scale of the catalyzed chemical reaction. They reflect the conformational changes that generate transition-state configurations conducive to the chemical reaction and thereby influence the activation free-energy barrier. Recently, conformational fluctuations of an enzyme active site occurring on the time scale of substrate turnover (i.e., hundreds of microseconds) have been identified with nuclear magnetic resonance (NMR) relaxation experiments (*62*).

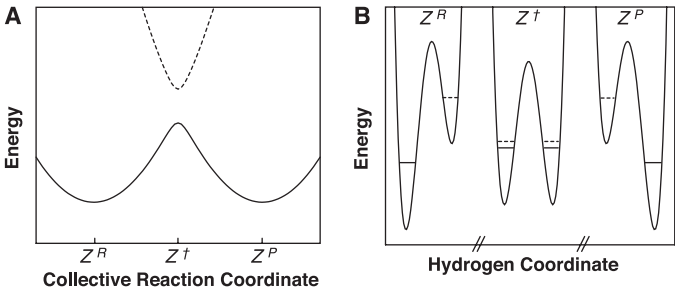

Fig. 4. Schematic illustration of a general hydrogen-transfer reaction. (**A**) Adiabatic vibrational free-energy curves as functions of a collective reaction coordinate. The solid curve represents the vibrational ground state, and the dotted curve represents the first excited vibrational state. (**B**) Hydrogen potential energy curves as functions of the hydrogen coordinate for three values of the reaction coordinate specified in part A. The Z^R, $Z^\dagger$, and Z^P values of the collective reaction coordinate represent the reactant, transition state, and product, respectively. The hydrogen coordinate spans a range of ≈1 Å for each potential energy curve. The ground and excited vibrational quantum states are represented by solid and dotted lines, respectively. The collective reaction coordinate determines the shape of the hydrogen potential energy curve and the relative energies of the hydrogen vibrational quantum states. The reorganization of the environment leads to nearly degenerate delocalized quantum states [corresponding to the top of the barrier in (A) with collective reaction coordinate $Z^\dagger$], thereby allowing hydrogen tunneling. The probability of hydrogen tunneling is determined by the height and width of the hydrogen-transfer barrier shown in the middle curve of (B).

Chemical reactions involving the transfer of light particles such as electrons and hydrogen nuclei may occur through quantum mechanical tunneling. There are many examples of enzyme-catalyzed processes of this type (*59*–*61*, *63*–*70*). According to Marcus theory (*71*), the collective reaction coordinate for electron transfer is comprised of the nuclear motions that influence the relative stabilities of the two charge-transfer states. Electron tunneling can occur when fluctuations of the nuclei lead to a configuration for which the two states are degenerate. The analogous mechanism has been proposed for hydrogen transfer, including proton and hydride transfer, as shown in Fig. 4 (*14*, *35*, *72*–*74*). In this case, the transferring hydrogen nucleus is viewed as a quantum mechanical wave function, and the collective reaction coordinate is comprised of motions of the heavy nuclei (*75*). The probability of hydrogen tunneling depends on the width and height of the hydrogen-transfer barrier, as determined by the configuration of the heavy atoms. A transition state for tunneling reactions can be defined to be the configuration at the top of the free-energy barrier along the collective reaction coordinate discussed in (*38*) (i.e., the heavy-atom configuration at which the two diabatic quantum states are degenerate, $Z^\dagger$ in Fig. 4). The rates for quantum mechanical tunneling reactions can be determined with the rate expressions mentioned above (*37*, *76*). In general, nuclear quantum effects may influence both the free-energy barrier and the barrier recrossings in hydrogen-transfer reactions (*64*, *76*).

Enzyme motion for reactions involving quantum mechanical tunneling has been discussed in terms of two distinct types of effects (*66*). First, the motion can alter the probability of achieving configurations with degenerate quantum states and, second, the motion can alter the probability of tunneling at this degenerate configuration (*77*). A number of researchers have discussed the importance of the second type of motion in electron and hydrogen-transfer reactions (*66*, *68*, *69*, *78*, *79*). These types of enzyme motions directly modulate the tunneling barrier, typically increasing the rate by decreasing the width and height of the barrier along the tunneling coordinate. Several terms have been used to describe this phenomenon, including "vibrationally enhanced tunneling" (*78*), "rate-promoting vibrations" (*69*), and "gating" (*66*). These types of motions are subpicosecond vibrations and hence are much faster than the chemical turnover of the enzyme reaction. Although the subpicosecond gating vibrations are critical for the modulation of the tunneling barrier, the equilibrium conformational changes along the collective reaction coordinate (i.e., the progression from Z^R to $Z^\dagger$ in Fig. 4) are thought to be rate-limiting (*69*). The dominant gating mode for a hydrogen-transfer reaction corresponds to the hydrogen donor-acceptor motion (*35*, *66*, *73*), which may influence both the activation free-energy barrier and the prefactor in the rate expressions (*37*, *80*). The underlying principles of the quantum mechanical tunneling process are the same in solution and enzymes, and quantification of the catalytic role of tunneling and gating vibrations is difficult (39). Further studies are required to quantify

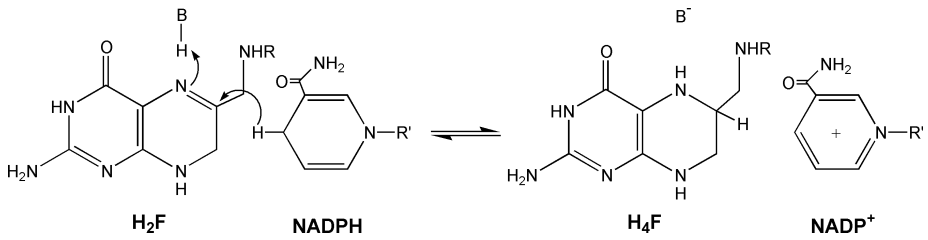

Fig. 5. The reaction catalyzed by DHFR. The reactant substrate is H_2F (dihydrofolate), the product substrate is H_4F (tetrahydrofolate), and the cofactor is NADPH/$NADP^+$ (nicotinamide adenine dinucleotide phosphate).

the catalytic role of tunneling and gating modes in enzymatic reactions.

A Case History

Dihydrofolate reductase (DHFR) catalyzes the reduction of 7,8-dihydrofolate (H_2F) to 5,6,7,8-tetrahydrofolate (H_4F) through a stereospecific transfer of the pro-*R* hydrogen from the cofactor nicotinamide adenine dinucleotide phosphate (NADPH) to C6 of the pterin nucleus with concurrent protonation at the N5 position (Fig. 5) (*81*). Because of its importance in the maintenance of intracellular levels of H_4F, which in turn is required for the biosynthesis of purines, pyrimidines, and several amino acids, the enzyme has been the target of important antineoplastic and antimicrobial drugs. Consequently, DHFR has been extensively studied with a wide range of methodologies.

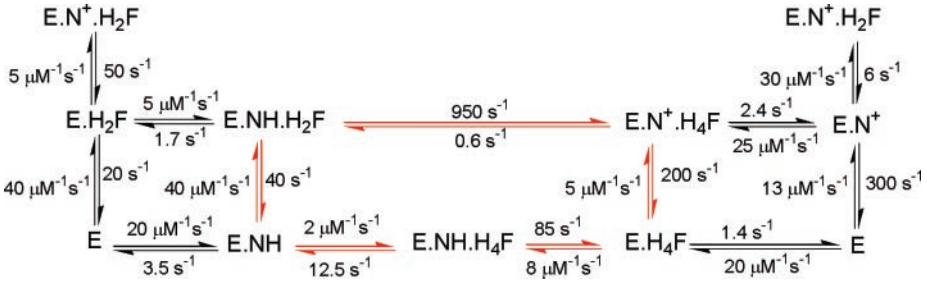

Fig. 6. The pH-independent kinetic scheme for DHFR catalysis at 25°C. E, DHFR; NH, NADPH; N^+, $NADP^+$; H_2F, dihydrofolate; and H_4F, tetrahydrofolate (*10*). The preferred pathway during multiple turnovers is shown in red.

Particularly pertinent to our discussion is the elucidation of the kinetic scheme for DHFR through presteady-state and steady-state kinetic analysis and of its structural features (in the presence and absence of ligands) through x-ray crystallography (*82*, *83*). The kinetic scheme shown in Fig. 6 provides a basis set for examining the properties of mutant forms of the enzyme and is characterized by a turnover cycle that involves the enzyme cycling among five kinetically observable species. Rapid hydride transfer within (E·NH·H_2F) produces E·N^+·H_4F at 950 s^{-1}, followed by $NADP^+$/NADPH exchange and rate-limiting loss of H_4F.

The structure of the ternary Michaelis complex E·NH·H_2F, which was modeled from the various complexes, is shown in Fig. 7. Prominent structural features include an eight-stranded β sheet and four α helices interspersed with loop regions that connect these structural elements. These flexible loops emanate from a rigid subdomain and include the Met^{20} loop, the βF-βG loop, and the βG- βH loop. In the presence of substrate or substrate analogs, the Met^{20} loop adopts a closed conformation, stabilized by hydrogen-bonding interactions with the βF-βG loop (residues 117 to 131). Specifically, the amide backbone of both Gly^{15} and Glu^{17} in the Met^{20} loop form hydrogen bonds with Asp^{122} in the βF- βG loop, bonds that are not present in the alternative occluded and open conformations of the Met^{20} loop. Juxtaposed to the loop subdomain is a larger subdomain that binds the adenosine portion of NADPH, and the two domains together form the active-site cleft. Its volume, similarly, is modulated by substrate binding, where subdomain movement sandwiches the *p*-aminobenzoyl glutamate side chain of H_2F between amino acid contacts arising from helix B and helix C. The net result is a closed conformation, as depicted in Fig. 7, that provides a preorganized structure that juxtaposes the substrate and coenzyme in an orientation conducive to reaction (*84*).

NMR relaxation experiments measuring the frequency and amplitude of amide backbone motions for the enzyme with bound folate, where the Met^{20} loop occludes the $NADP^+$ binding site as expected for a product conformation, found four notable regions of enhanced flexibility: the Met^{20} loop (residues 16 to 22), the adenosine binding loop (residues 67 to 69), the hinge regions (residues 38 and 88), and the βF- βG loop (residues 119 to 123) (*85*). Subsequent studies on surrogate substrate and product ternary complexes showed that, for example, in the DHFR·$NADP^+$ folate complex (a representative of the Michaelis complex with the Met^{20} loop in a closed conformation) the nanosecond-picosecond scale backbone dynamics within these regions are attenuated, consistent with the structural consequences of ligand binding. The identification by NMR of key residues—both proximal and distal to the active site—that are highly motional and furthermore that are conserved across 36 diverse species of DHFR from *E. coli* to human, suggested the key participation of these residues in the catalytic cycle (*86*). Particularly intriguing is how residues not in direct contact with, nor apparently capable of sufficient conformational movement to achieve contact with, active-site ligands are able to influence catalysis (*60*). Recent single-molecule experiments have also indicated the importance of protein conformational changes, particularly the motion of the Met^{20} loop (*87*).

Extensive studies of site-directed mutants have substantiated the importance of many of these conserved residues distributed throughout the protein. For example, substitution of Gly^{121} in the βF-βG loop with valine decreases the rate of hydride transfer by a factor of 200; mutagenesis of the highly conserved Met^{42} to Phe reduces this rate by a factor of 1.5, but in combination with a second mutation at Gly^{121} (M42F, G121A) slows the rate of the hydride transfer step by a factor of 20 more than expected if the individual effects on the rate were additive (*88*, *89*). One may argue, of course, that the decrease in enzyme

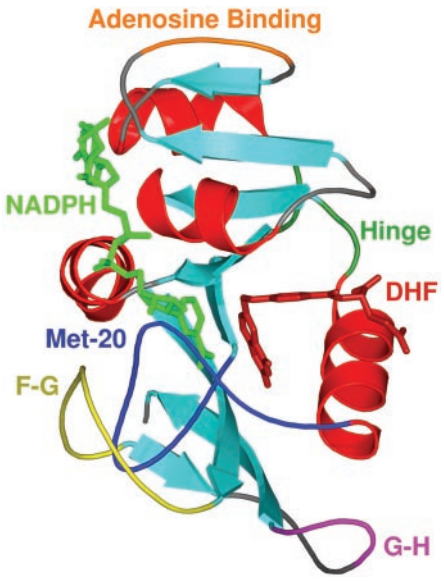

Fig. 7. Secondary structure of DHFR. The Met^{20}, βF-βG, βG-βH, and adenosine binding loops, the hinge regions, the NADPH cofactor, and the DHF substrate are labeled (*60*).

activity is the result of subtle perturbations in the enzyme's structure not readily measured by conventional structure analysis (single-site mutations are generally localized in their perturbation of protein structure to the point of the amino acid substitution) (*89*). If so, one is still left with the question as to how the effect is transmitted over distances approaching 20 Å for DHFR.

We turned to theory to address these issues. Classical molecular dynamics simulations for up to 10 ns on various DHFR complexes provided residue-residue–based maps of correlated motions in the backbone. These maps indicated strong correlated and anticorrelated motions involving spatially distinct regions, many of which were in the same regions of the protein identified in the dynamic NMR measurements. These correlations were found in the reactant but not in the product ternary complexes. Moreover, these regions generally encompassed the proximal and distal residues whose substitution led to debilitating changes in the hydride transfer rate (*47*). When combined with the genomic sequence conservation data (*60*), a conserved set of residues emerged that may act to facilitate hydride transfer.

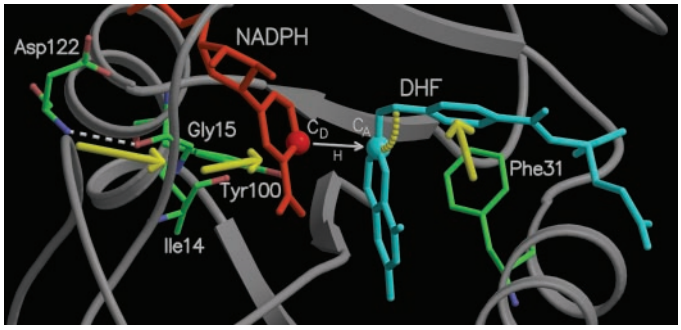

Fig. 8. Schematic diagram of a portion of a network of coupled promoting motions in DHFR. The yellow arrows and arc indicate the coupled promoting motions. This picture does not represent a complete or unique network but rather illustrates the general concept of reorganization of the enzymatic environment to provide configurations conducive to the hydride transfer reaction. Reproduced from (*60*).

Hybrid quantum-classical molecular dynamics simulations of the hydride transfer reaction catalyzed by DHFR have provided further information about enzyme motion in DHFR (*60*, *61*). These hybrid simulations were used to identify thermally averaged motions that influence the activation free-energy barrier and dynamical motions that influence the barrier recrossings. For reasons discussed above, the thermally averaged motions influencing the activation free-energy barrier are expected to have a greater impact on enzymatic activity than do the dynamical motions influencing the barrier recrossings. These thermal motions are averaged over the fast vibrations and reflect conformational changes occurring along the collective reaction coordinate on the time scale of the catalyzed chemical reaction (i.e., the reorganization of the enzymatic environment leading to configurations with degenerate hydride transfer quantum states, from Z^R to $Z^\dagger$ in Fig. 4). The hybrid simulations provide evidence for a network of coupled promoting motions extending throughout the protein and ligands (Fig. 8), where promoting motions refer to equilibrium, thermally averaged conformational changes along the collective reaction coordinate leading to configurations conducive to the reaction (*90*). Hybrid simulations of the G121V mutant discussed above are consistent with the experimental rate measurements and suggest that the mutation may modify the network of coupled motions through structural perturbations, thereby increasing the free-energy barrier and decreasing the reaction rate (*91*). The equilibrium molecular motions in this network are not dynamically coupled to the chemical transformation of the substrate and cofactor, but rather give rise to conformations of the ternary complex in which the hydride transfer reaction is facilitated because of short transfer distances, suitable orientation of substrate and cofactor, energetic matching of diabatic charge-transfer states, and a favorable electrostatic environment for charge transfer. A recent study (*92*) on DHFR using different computational methods has generated qualitatively similar results.

Implications

One may, of course, immediately question whether the coupled network of our case history can be generalized. With the advent of genomic sequencing and rapid structure determination, the outlines of the "protein universe" (in terms of sequence space, infinite, in terms of protein folds, ~650 to ~10,000) have become visible. Classifying proteins into families (*93*) (significant sequence similarity and conservation of function) and superfamilies (reduced sequence similarity but recognizable, conserved motifs and conservation of function) found the majority distributed unevenly over ~1000 folds (*94*–*96*). Although the chemical reactions catalyzed by enzymes in superfamilies may differ, they generally retain a common mechanistic element manifest in a reaction-intermediate or key transition state (*97*, *98*).

In the analyses of superfamilies constructed from a common fold, one generally finds absolutely conserved functional residues situated within a superimposable topological framework. One may ask whether there is also residue conservation in other elements of the secondary structure for family proteins. Within families, indeed, persistently conserved positions are found. With correlated mutation analyses, functionally (*99*, *100*) important residues may be extracted. In many cases, the conservation (*101*) of the location of the residue appears more important than residue type at a particular position. Although these amino acids may be important in the maintenance of structure, their roles may also include participation in a regulatory mechanism involving the binding of modifiers and the transmission of the effect to the active site (*102*). We would add to that list their participation in a coupled network for optimal catalytic efficiency.

Correlated networks have been found in globins involved in heme binding and in the α/β subunit interface linked to the cooperativity of the globins; in serine esterases, including the active-site residues, calcium binding site, and in linking this latter site to other regions of the protein; and in G protein–coupled receptor proteins linking guanosine triphosphate binding to signaling switch regions. Correlation analysis on DHFR finds conserved residues, among others, that link the βF-βG loop region and NADPH binding site despite the divergence in sequence to less than 30% identity (*103*).

Confounding these analyses, however, are more examples of related enzymes in which different functional groups, unconserved with respect to position in the primary sequence, provide an alternative solution to catalyzing a given reaction. Examples include the enolase/mandelate pair, where the locus of a key lysine has been altered, and the DD-peptidase/β-lactamase pair, where the acid-base catalysts are donated by differing secondary structures elements.

This active-site plasticity has been exploited in rational strategies to reshape enzyme specificities where often single substitutions change a substrate specificity. Linoleate 13-lipoxygenase, for example, is changed to a 9-lipoxygenating species by a His^{608} Val mutation that demasks a positive charge at the bottom of the active site and changes the orientation of the fatty-acid substrate (*104*). In a more extreme example, a stretch of 13 amino acids within the active site of *Thermus aquaticus* DNA polymerase I was extensively randomly mutated, giving rise to a library of ~8,000 active mutants. Several mutants show polymerase activity higher than that of wild-type enzyme (*105*), and others have the ability to incorporate

ribonucleotide analogs. On the other hand, manipulating the specificity of aspartate aminotransferase (*106*) to favor valine (k_{cat}/K_M is increased 10^6-fold) required changes in 17 amino acids, only one of which is within the active site (*107*).

A similar lesson is taught repeatedly by natural evolution. For example, methionyl amino peptidase, which catalyzes the removal of the amino-terminal leader methionine residue from polypeptides, and creatinase, which promotes the hydrolysis of creatine to sarcosine and ammonia, apparently diverged from a common ancestor and represent an unusual case in which specificity and catalytic mechanism differ (the peptidase uses a metal ion; the hydrolase does not). The common core of the homologous (*108*) fold consists of ~180 structurally equivalent and 39 identical sites.

We propose that in all these cases there is retention of key coupled networks whose role among others is to provide a framework for maintaining catalytic optimal activity. Active-site residue redundancy as well as plasticity then can be accommodated. Violation of such networks by mutagenesis would act to diminish catalytic activity, even if the fold were preserved. One may speculate that the failure to reshape trypsin into chymotrypsin may stem from that type of violation (*109*). On the other hand, the success of domain swapping to create chimeric restriction enzymes (various DNA binding motifs fused to a DNA cleavage domain) and of shuffling amino acid sequences of high homology to form enzyme hybrids may reflect intact transfer of protein sequences for recreation of such a coupled network (*110*, *111*). The concept of coupled networks also has been applied to the origin and evolution of enzymes in metabolic pathways, where analysis of genomic sequence finds block sequence conservation that occurs in enzymes sharing similar substrate structures (adjacent or less than three steps distant) in metabolic pathways (*112*).

Conclusion

The exploration for links between protein structure, movement, and catalysis will be expanded by the advent of new methods. We anticipate additional examples of enzymes for which motion is important and other cases for which it is not. Particularly attractive are techniques that permit the observation of single molecules on the same millisecond-to-second time scale on which enzymatic reactions normally occur. Such kinetics provide data for conformational changes during enzymatic turnover that may be masked in ensemble-averaged studies (*87*, *113*). Ensemble studies featuring isotopic editing of specific regions of the protein coupled with temperature jump relaxation also show considerable promise in detecting motions of mobile loops and active-site residues important to catalysis (*114*). Similarly, the extensive isotopic labeling of the substrate coupled with kinetic isotope effect analysis can provide structural information for reaction coordinate motions from the vantage point of the substrate (*63*, *115*). Isotopic editing, of course, remains the basis of Raman, infrared, and NMR studies of protein dynamics. High-resolution x-ray crystallographic structures mapping progressive conformational changes in a multistep reaction sequence can now be rapidly solved (*116*). In addition, the continued development of more sophisticated theoretical and computational tools will enable more definitive calculations on enzymatic processes. The symbiotic marriage of experiment and theory is vital for the elucidation of a complete picture of enzyme catalysis.

References and Notes

1. E. Fischer, *Ber. Dtsch. Chem. Ges.* **27**, 3189 (1894).
2. J. B. S. Haldane, *Enzymes* (Longmans, Green, London, 1930).
3. L. Pauling, *Nature* **161**, 707 (1948).
4. C. C. Blake *et al.*, *Nature* **206**, 757 (1965).
5. M. F. Perutz, *Faraday Discuss. Chem. Soc.* **93**, 1 (1992).
6. A. Warshel, M. Levitt, *J. Mol. Biol.* **103**, 227 (1976).
7. R. Wolfenden, C. Ridgway, G. Young, *J. Am. Chem. Soc.* **120**, 833 (1998).
8. R. Wolfenden, M. J. Snider, C. Ridgway, B. Miller, *J. Am. Chem. Soc.* **121**, 7419 (1999).
9. A. Radzicka, R. Wolfenden, *Science* **267**, 90 (1995).
10. W. R. Cannon, S. J. Benkovic, *J. Biol. Chem.* **273**, 26257 (1998).
11. R. D. Gandour, R. L. Schowen, Eds., *Transition States of Biochemical Processes* (Plenum, New York, 1978).
12. W. Zhong, S. J. Benkovic, *Anal. Biochem.* **255**, 66 (1998).
13. W. R. Cannon, S. F. Singleton, S. J. Benkovic, *Nature Struct. Biol.* **3**, 821 (1996).
14. A. Warshel, *Proc. Natl. Acad. Sci. U.S.A.* **81**, 444 (1984).
15. F. H. Westheimer, *Adv. Phys. Org. Chem.* **21**, 1 (1985).
16. W. P. Jencks, *Chem. Rev.* **72**, 705 (1972).
17. T. C. Bruice, *Annu. Rev. Biochem.* **45**, 331 (1976).
18. K. Tanabe, G. McKay, J. D. Payzant, D. Bohme, *Can. J. Chem.* **54**, 1643 (1976).
19. M. J. Dewar, D. M. Storch, *Proc. Natl. Acad. Sci. U.S.A.* **82**, 2225 (1985).
20. M. F. Perutz, *Proc. R. Soc. London Ser. B* **167**, 448 (1967).
21. G. E. Lienhard, *J. Am. Chem. Soc.* **88**, 5642 (1966).
22. A. Warshel, *Proc. Natl. Acad. Sci. U.S.A.* **75**, 5250 (1978).
23. J. R. Knowles, *Nature* **350**, 121 (1991).
24. The alert reader will note that the imidazole of His^{95} acts as a general acid in its free-base form.
25. T. C. Bruice, U. K. Pandit, *J. Am. Chem. Soc.* **82**, 5858 (1960).
26. W. P. Jencks, *Adv. Enzym.* **43**, 219 (1975).
27. T. C. Bruice, *Acc. Chem. Res.* **35**, 139 (2002).
28. A. Shurki, M. Strajbl, J. Villa, A. Warshel, *J. Am. Chem. Soc.* **124**, 4097 (2002).
29. G. G. Hammes, *Nature* **204**, 342 (1964).
30. D. E. Koshland Jr., K. E. Neet, *Annu. Rev. Biochem.* **37**, 359 (1968).
31. Typically, electronically (vibrationally) adiabatic refers to reactions occurring in the electronic (vibrational) ground state, whereas electronically (vibrationally) nonadiabatic refers to reactions involving excited electronic (vibrational) states. The adiabatic limit corresponds to strong coupling and the nonadiabatic limit corresponds to weak coupling between the charge-transfer states.
32. D. Chandler, *J. Stat. Phys.* **42**, 49 (1986).
33. B. J. Gertner, K. R. Wilson, J. T. Hynes, *J. Chem. Phys.* **90**, 3537 (1989).
34. P. F. Barbara, T. J. Meyer, M. A. Ratner, *J. Phys. Chem.* **100**, 13148 (1996).
35. D. Borgis, J. T. Hynes, *Chem. Phys.* **170**, 315 (1993).
36. A. M. Kuznetsov, J. Ulstrup, *Can. J. Chem.* **77**, 1085 (1999).
37. The nonadiabatic rate is a sum of products of a prefactor and an exponential of a free-energy barrier, where the summation is over all relevant reactant and product quantum states. The prefactor differs in the adiabatic and nonadiabatic limits. For nonadiabatic electron and hydrogen-transfer reactions, the prefactor includes the coupling matrix element between the reactant and product wave functions, which determines the tunneling probability.
38. The assumption of a single reaction coordinate may not be appropriate for all types of reactions (e.g., multiple charge-transfer reactions). Furthermore, the choice of reaction coordinate is not unique. In some descriptions, the transition state is a saddle point on the coordinate potential energy surface, and the collective reaction coordinate corresponds to the minimum energy path from the transition state to the reactant and product. In alternative descriptions, the transition state is not necessarily a saddle point on the coordinate potential energy surface. For example, the collective reaction coordinate for charge-transfer reactions can be defined as the difference in the energies of two charge-transfer states interacting with the environment, and the transition state corresponds to the configuration at which this energy reaction coordinate is zero (*39*, *64*, *71*, *74*).
39. J. Villa, A. Warshel, *J. Phys. Chem. B* **105**, 7887 (2001).
40. H. Frauenfelder, P. G. Wolynes, *Science* **229**, 337 (1985).
41. C. L. Tsou, *Science* **262**, 380 (1993).
42. L. Young, C. B. Post, *Biochemistry* **35**, 15129 (1996).
43. H. X. Zhou, S. T. Wlodek, J. A. McCammon, *Proc. Natl. Acad. Sci. U.S.A.* **95**, 9280 (1998).
44. I. Bahar, B. Erman, R. L. Jernigan, A. R. Atilgan, D. G. Covell, *J. Mol. Biol.* **285**, 1023 (1999).
45. E. Freire, *Proc. Natl. Acad. Sci. U.S.A.* **97**, 11680 (2000).
46. H. Pan, J. C. Lee, V. J. Hilser, *Proc. Natl. Acad. Sci. U.S.A.* **97**, 12020 (2000).
47. J. L. Radkiewicz, C. L. I. Brooks, *J. Am. Chem. Soc.* **122**, 225 (2000).
48. M. Karplus, *J. Phys. Chem. B* **104**, 11 (2000).
49. S. Caratzoulas, S. D. Schwartz, *J. Chem. Phys.* **114**, 2910 (2001).
50. S. Piana, P. Carloni, M. Parrinello, *J. Mol. Biol.* **319**, 567 (2002).
51. Q. Cui, M. Karplus, *J. Phys. Chem. B* **106**, 7927 (2002).
52. B. D. Dunietz *et al.*, *J. Am. Chem. Soc.* **122**, 2828 (2000).
53. D. S. Lu, G. A. Voth, *Proteins Struct. Funct. Genet.* **33**, 119 (1998).
54. D. Suarez, E. Brothers, K. M. Merz, *Biochemistry* **41**, 6615 (2002).
55. S. Hammes-Schiffer, *Biochemistry* **41**, 13335 (2002).
56. M. Karplus, J. D. Evanseck, D. Joseph, P. A. Bash, M. J. Field, *Faraday Discuss. Chem. Soc.* **93**, 239 (1992).
57. J. L. Gao, *Curr. Opin. Struct. Biol.* **13**, 184 (2003)
58. J. K. Hwang, Z. T. Chu, A. Yadav, A. Warshel, *J. Phys. Chem.* **95**, 8445 (1991).
59. S. R. Billeter, S. P. Webb, P. K. Agarwal, T. Iordanov, S. Hammes-Schiffer, *J. Am. Chem. Soc.* **123**, 11262 (2001).
60. P. K. Agarwal, S. R. Billeter, P. T. R. Rajagopalan, S. J. Benkovic, S. Hammes-Schiffer, *Proc. Natl. Acad. Sci. U.S.A.* **99**, 2794 (2002).
61. P. K. Agarwal, S. R. Billeter, S. Hammes-Schiffer, *J. Phys. Chem. B* **106**, 3283 (2002).
62. E. Z. Eisenmesser, D. A. Bosco, M. Akke, D. Kern, *Science* **295**, 1520 (2002).
63. Y. Cha, C. J. Murray, J. P. Klinman, *Science* **243**, 1325 (1989).
64. S. R. Billeter, S. P. Webb, T. Iordanov, P. K. Agarwal, S. Hammes-Schiffer, *J. Chem. Phys.* **114**, 6925 (2001).
65. D. G. Truhlar *et al.*, *Acc. Chem. Res.* **35**, 341 (2002).

66. M. J. Knapp, K. Rickert, J. P. Klinman, *J. Am. Chem. Soc.* **124**, 3865 (2002).
67. M. J. Knapp, J. P. Klinman, *Eur. J. Biochem.* **269**, 3113 (2002).
68. M. J. Sutcliffe, N. S. Scrutton, *Eur. J. Biochem.* **269**, 3096 (2002).
69. D. Antoniou, S. Caratzoulas, C. Kalyanaraman, J. S. Mincer, S. D. Schwartz, *Eur. J. Biochem.* **269**, 3103 (2002).
70. S. Chowdhury, R. Banerjee, *J. Am. Chem. Soc.* **122**, 5417 (2000).
71. R. A. Marcus, N. Sutin, *Biochim. Biophys. Acta* **811**, 265 (1985).
72. S. Hammes-Schiffer, J. C. Tully, *J. Chem. Phys.* **101**, 4657 (1994).
73. D. Borgis, J. T. Hynes, *J. Phys. Chem.* **100**, 1118 (1996).
74. K. Ando, J. T. Hynes, *J. Mol. Liq.* **64**, 25 (1995).
75. For a two-state model of electron transfer, the electron is localized on the donor for state 1 and on the acceptor for state 2. For the analogous two-state model of hydrogen transfer, the hydrogen vibrational wave function is localized near the donor for state 1 and near the acceptor for state 2. The motion of the heavy nuclei leads to a configuration for which the two states are degenerate. For hydrogen-transfer reactions, the hydrogen may tunnel at this degenerate configuration. If the vibrational ground state is above the hydrogen-transfer barrier, or this barrier is zero, the reaction is not called "tunneling" but is still quantum mechanical in nature.
76. Simulation approaches in which a tunneling "correction" is included in the prefactor (*65*, *117*, *118*) are useful for certain hydrogen-transfer systems but may be problematic in other regimes (*67*). An alternative approach (*64*) includes nuclear quantum mechanical effects for the calculation of the free-energy barrier, as well as for the calculation of the transmission coefficient prefactor. In this approach, the transition-state theory rate constant represents the adiabatic rate, and the transmission coefficient accounts for nonadiabatic effects as well as dynamical barrier recrossings. In this case (*64*), the transmission coefficient is between zero and unity, whereas tunneling corrections (*65*, *117*, *118*) introduce a prefactor that may be greater than unity.
77. These two effects are not rigorously separable in the enzyme reaction, and many enzyme motions contribute to both types of effects. Moreover, there is not a one-to-one correspondence between these two effects and the free-energy barrier and transmission coefficient.
78. W. J. Bruno, W. Bialek, *Biophys. J.* **63**, 689 (1992).
79. I. Daizadeh, E. S. Medvedev, A. A. Stuchebrukhov, *Proc. Natl. Acad. Sci. U.S.A.* **94**, 3703 (1997).
80. For hydrogen-transfer reactions, the hydrogen donor-acceptor vibrational mode can be either included in the collective reaction coordinate representing the reorganization of the environment in Fig. 4 (*64*) or treated separately from the other motions in the enzyme system (*66*). The equilibrium, thermally averaged value of the donor-acceptor distance has been shown to change substantially along the collective reaction coordinate for hydrogen-transfer reactions (*59*, *61*).
81. P. A. Charlton, D. W. Young, B. Birdsall, J. Feeney, G. C. K. Roberts, *J. Chem. Soc. Chem. Commun.* 922 (1979).
82. C. A. Fierke, K. A. Johnson, S. J. Benkovic, *Biochemistry* **26**, 4085 (1987).
83. M. R. Sawaya, J. Kraut, *Biochemistry* **36**, 586 (1997).
84. T. C. Bruice, S. J. Benkovic, *Biochemistry* **39**, 6267 (2000).
85. D. M. Epstein, S. J. Benkovic, P. E. Wright, *Biochemistry* **34**, 11037 (1995).
86. M. J. Osborne, J. Schnell, S. J. Benkovic, H. J. Dyson, P. E. Wright, *Biochemistry* **40**, 9846 (2001).
87. P. T. R. Rajagopalan *et al.*, *Proc. Natl. Acad. Sci. U.S.A.* **99**, 13481 (2002).
88. G. P. Miller, S. J. Benkovic, *Chem. Biol.* **5**, R105 (1998).
89. P. T. R. Rajagopalan, S. Lutz, S. J. Benkovic, *Biochemistry* **41**, 12618 (2002).
90. Note that the network of coupled motions identified from the simulations is most likely not complete or unique, and the analysis is unable to differentiate between motions playing an active role in catalysis and motions responding to alterations caused by catalysis. Moreover, the details of this network may depend on the potential energy surface and sampling procedure implemented in the simulations.
91. J. B. Watney, P. K. Agarwal, S. Hammes-Schiffer, *J. Am. Chem. Soc.* **125**, 3745 (2003).
92. T. H. Rod, J. L. Radkiewicz, C. L. Brooks III, *Proc. Natl. Acad. Sci. U.S.A.* **100**, 6980 (2003).
93. E. V. Koonin, Y. I. Wolf, G. P. Karev, *Nature* **420**, 218 (2002).
94. L. Holm, C. Sander, *Science* **273**, 595 (1996).
95. A. G. Murzin, *Curr. Opin. Struct. Biol.* **6**, 386 (1996).
96. A. E. Todd, C. A. Orengo, J. M. Thornton, *J. Mol. Biol.* **307**, 1113 (2001).
97. J. A. Gerlt, P. C. Babbitt, *Curr. Opin. Chem. Biol.* **2**, 607 (1998).
98. P. C. Babbitt, J. A. Gerlt, *J. Biol. Chem.* **272**, 30591 (1997).
99. I. Friedberg, H. Margalit, *Protein Sci.* **11**, 350 (2002).
100. L. A. Mirny, E. I. Shakhnovich, *J. Mol. Biol.* **291**, 177 (1999).
101. L. Oliveira, A. C. M. Paiva, G. Vriend, *J. Comput. Aided Mol. Des.* **7**, 649 (1993).
102. S. W. Lockless, R. Ranganathan, *Science* **286**, 295 (1999).
103. G. L. Moore, C. D. Maranas, *Proc. Natl. Acad. Sci. U.S.A.* **100**, 5091 (2003).
104. E. Hornung, M. Walther, H. Kuhn, I. Feussner, *Proc. Natl. Acad. Sci. U.S.A.* **96**, 4192 (1999).
105. P. H. Patel, L. A. Loeb, *Proc. Natl. Acad. Sci. U.S.A.* **97**, 5095 (2000).
106. E. Deu, K. A. Koch, J. F. Kirsch, *Protein Sci.* **11**, 1062 (2002).
107. S. Oue, A. Okamoto, T. Yano, H. Kagamiyama, *J. Biol. Chem.* **274**, 2344 (1999).
108. A. G. Murzin, *Trends Biochem. Sci.* **18**, 403 (1993).
109. J. J. Perona, C. S. Craik, *J. Biol. Chem.* **272**, 29987 (1997).
110. S. Chandrasegaran, J. Smith, *Biol. Chem. Hoppe-Seyler* **380**, 841 (1999).
111. J. Minshull, W. P. Stemmer, *Curr. Opin. Chem. Biol.* **3**, 284 (1999).
112. R. Alves, R. A. Chaleil, M. J. Sternberg, *J. Mol. Biol.* **320**, 751 (2002).
113. X. S. Xie, H. P. Lu, *J. Biol. Chem.* **274**, 15967 (1999).
114. R. Callender, R. B. Dyer, *Curr. Opin. Struct. Biol.* **12**, 628 (2002).
115. A. Fedorov *et al.*, *Biochemistry* **40**, 853 (2001).
116. R. M. Stroud, J. Finer-Moore, *Biochemistry* **42**, 239 (2003).
117. R. P. Bell, *The Tunneling Effect in Chemistry* (Chapman & Hall, London and New York, 1980).
118. C. Alhambra, J. C. Corchado, M. L. Sanchez, J. Gao, D. G. Truhlar, *J. Am. Chem. Soc.* **122**, 8197 (2000).
119. J. M. Thomas, *Angew. Chem. Int. Ed. Eng.* **33**, 913 (1994).
120. J. A. McCammon, S. C. Harvey, *Dynamics of Proteins and Nucleic Acids* (Cambridge Univ. Press, New York, 1987).
121. G. G. Hammes, *Biochemistry* **41**, 8221 (2002).

122. S.J.B. acknowledges funding from NIH grants GM13306 and GM24129. S.H.-S. acknowledges funding from NIH grant GM56207 and NSF grant CHE-0096357. We also thank Yolanda Small and James Watney for creating the figures.